On Using Functions to Describe the Shape

VOLODYMYR V. KINDRATENKO
*National Center for Supercomputing Applications (NCSA), University of Illinois at Urbana-Champaign (UIUC),
405 North Mathews Avenue, Urbana, IL 61801, USA*
kindr@ncsa.uiuc.edu

Abstract. In this paper, a systematic review of various contour functions and methods of their analysis, as applied in the field of shape description and characterization, is presented. Contour functions are derived from planar object outlines and are used as an intermediate representation from which various shape properties can be obtained. All the functions are introduced and analyzed following the same scheme, thus making it possible to compare various representations. Although only a small subset of contour functions is included in the survey (cross-section, radius-vector, support, width, parametric, complex, tangent-angle, curvature, polynomial, and parametric cubic), the paper demonstrates a multitude of techniques for shape description that are based on this approach. Several analysis tools, such as statistics, line moments and invariants, Fourier and other series expansions, curvature scale space image, wavelet, and Radon transform are described.

Keywords: contour functions, shape, shape analysis, 2D object recognition

1. Introduction

The problem of shape analysis has been given constant attention in pattern recognition and computer vision literature. The field has been intensively developed over past decades both in theoretical and applied domains [31]. Three major directions in shape analysis can be identified based on how the object, the shape of which is analyzed, is treated in mathematical terms [46]. In the *set theory* approach, elements of set theory are used to describe the objects. Shape analysis methods based on mathematical morphology and fractal geometry are examples of this approach. In the *functional* approach, functions are used to represent the shape. Such representation is possible in many ways and it results in a function that embeds desirable characteristics and properties of the shape. Theory of functions and differential geometry can be directly applied to study such shape functions. In the *statistical shape analysis* approach, the concept of replacing an object by a group of points that are constrained by some geometrical properties or have a certain physical meaning is exploited. Such "point fields" are analyzed by various statistical methods.

In this review, shape description methods based on functions are considered. Contour functions are appropriate for many applications because of their advantages over other methods [46]: (i) an effective data reduction—frequently only a few coefficients of the approximation function are needed for a rather precise form description, (ii) a convenient description of complex forms, and (iii) an intuitive characterization of many form properties that can be derived analytically and therefore are very accurate. The necessary choice of a reference point to be the origin that often appears to be arbitrary, and complicated analytical formulae for functions and characteristics even for simple shapes are among the disadvantages of this approach.

The shape of an object is a difficult concept. An ideal shape parameter is a set function value that does not depend on geometrical transformations such as translation, rotation, size changes and reflection. Here only *two-dimensional* objects or two-dimensional images of three-dimensional objects, which can be their projections or sections, are considered. It is assumed that the two-dimensional information is sufficient for a reasonable characterization. It is always assumed that the objects are sets in the sense of mathematical set

theory. It is assumed that the sets are compact and closed in the topological sense. Following the definition proposed in [46], such sets will be referred to as *figures*. The closure of the figure is called the *boundary*. The *contour* of a figure is a closed planar curve that consists of the elements of the figure boundary. When all the information in the figure about its location, scale, and orientation, is removed, the information that reminds is called the *shape* of the figure. In this review, only the continuous case is considered as it provides the basis for analyzing discretized contours. More on the specifics associated with the discretized curves can be found elsewhere [19, 25, 44, 52].

2.   Contour Functions

There are two basic principles that can be exploited to derive a contour function: symmetry and periodicity. If the contour of a figure is symmetric with respect to a line, the orthogonal distance of the contour point from the symmetry line as a function of position on the symmetry line can be considered as a contour function. Contour function may be periodic, the contour itself can be considered as a periodic function. Assuming that the contour has some desirable properties, such as convexity, relatively simple contour functions can be introduced. In a more general sense, the contour itself can be parameterized and treated as a function. Also, one contour function may be derived from another contour function.

2.1.   Cross-Section Function for Symmetric Figures

It is natural to describe the form of a symmetric figure by the cross-section function, the half-breadth at x [46]. Consider a symmetric figure that is oriented in such a way that its symmetry axis coincides with the x-axis of the coordinate system. Only one-half of the

figure is used and for each of its point the coordinates $(x, q_X(x))$ are obtained where $q_X(x)$ is the half-breadth at x (Fig. 1(a)). Problems occur if there is more than one contour point on the line through x orthogonal to the symmetry axis (Fig. 1(b)). This ambiguity can be removed by choosing the mean distance as the function value, or the outer contour point, or by smoothing the contour. These simplifications however may destroy essential features of the contour. Another problem occurs when a figure has more than one symmetry line. In this case, more than one cross-section function can exist. Examples of a symmetric figure and its cross-section function are given in Fig. 2.

The cross-section function $q_X(x)$ of figure X

1. is invariant under translation: $q_{X+v}(x) = q_X(x)$ where $X + v$ is X translated by a vector v;
2. depends on changes of the size of the figure: $q_{\lambda X}(x) = \lambda q_X(x)$ where λX is figure X zoomed by a factor λ;
3. does not depend on the orientation of the figure;
4. is, in general, not invariant under reflection;
5. is not periodic, in fact, it is defined only for a certain interval on x;
6. if figure X is a subset of figure Y ($X \subset Y$), then $q_X(x) \le q_Y(x)$.

Figure perimeter $P(X)$ and area $A(X)$ can be obtained by integrating its cross-section function $q_X(x)$:

$$P(X) = 2 \int_{x_0}^{x_1} \sqrt{1 + q_X'^2(x)} \, dx \text{ and}$$

$$A(X) = 2 \int_{x_0}^{x_1} q_X(x) \, dx.$$

2.2.   Radius-Vector Function

Frequently the contour of a figure is described by the *radius-vector function* defined in the following way
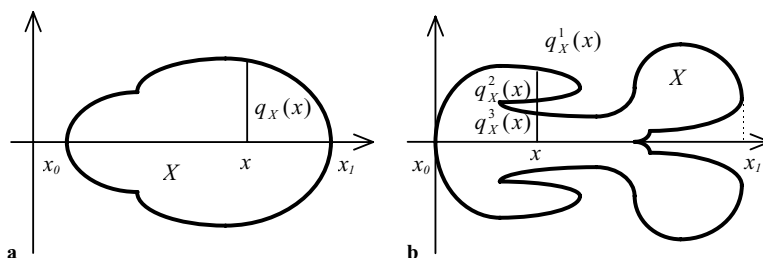

Figure 1.   (a) definition of the cross-section function for symmetric figures; (b) problems with the cross-section functions occur if there is more than one contour point on the line through x orthogonal to the symmetry axis.
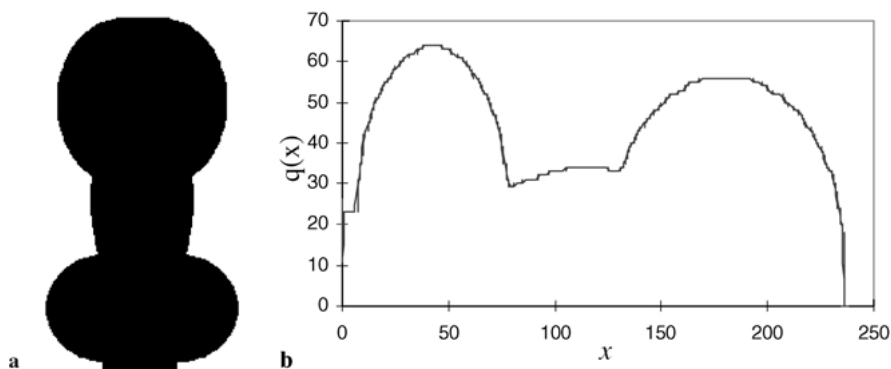
Figure 2. (a) symmetric figure X; (b) cross-section function $q_X(x)$ of figure X.
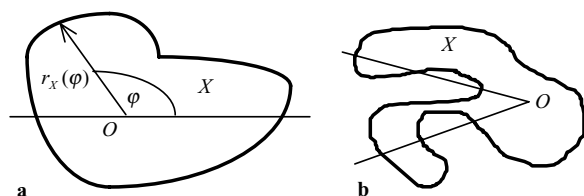

Figure 3. (a) definition of the radius-vector function; (b) problems with the radius-vector function occur if the figure is not star-shaped.

[10, 31, 32, 42, 46]. A reference point O in the interior of figure X is selected which is usually the center of gravity, or the center of the smallest disc which completely contains the figure, or a physically important point. Next, an appropriate reference line l crossing the reference point O is chosen which is usually parallel to the x- or y-axis. Then the radius-vector function $r_X(\varphi)$ is the distance from the reference point O to the contour in the direction of the φ-ray where $0 \leq \varphi \leq 2\pi$ (Fig. 3(a)).

It is necessary, however, that the figure is star-shaped with respect to O. That is, for any contour point p the whole line segment from O to p should lie within the figure. In this case, the radius-vector function completely characterizes the figure: if $r_X(\varphi)$ is given, then the figure can be uniquely reconstructed.

The figure can be star-shaped with respect to one reference point, even if it is not with respect to another. If the star-shapedness is violated by only small irregularities in the contour, it is possible to recover it by smoothing or by moving the reference point. In the general case however, description by the radius-vector function is not suitable for non-star-shaped figures. Examples of a star-shaped figure and its radius-vector function are given in Fig. 4.

The radius-vector function $r_X(\varphi)$ of a star-shaped figure X

1. is invariant under translation: $r_{X+v}(\varphi) = r_X(\varphi)$ where $X + v$ is X translated by a vector v;
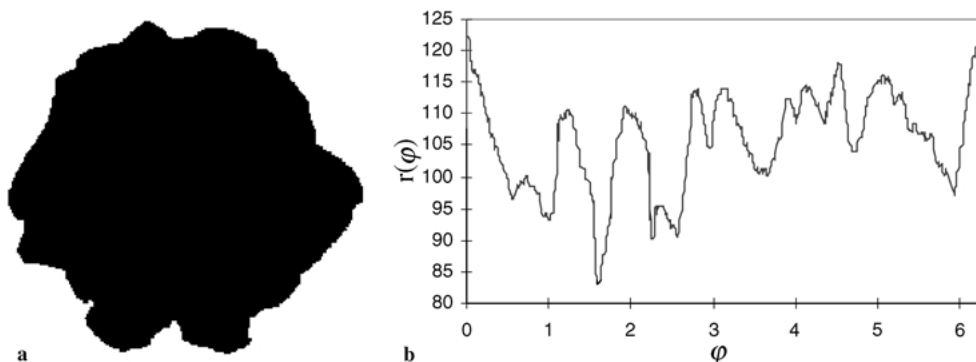

Figure 4. (a) start-shaped figure X; (b) radius-vector function $r_X(\varphi)$ of figure X. The center of gravity of the figure was used as the origin to generate the radius-vector function.

2. depends on the changes of the size of the figure: $r_{\lambda X}(\varphi) = \lambda r_X(\varphi)$ where λX is figure X zoomed by a factor λ;

3. depends on the orientation of the figure: $r_X(\varphi) = r_Y(\varphi - \alpha)$ where Y is figure X rotated by an angle α;

4. is not invariant under reflection;

5. is periodic with the period 2π: $r_X(\varphi + 2\pi) = r_X(\varphi)$;

6. if a start-shaped figure X is a subset of a star-shaped figure Y ($X \subset Y$), then $r_X(\varphi) \leq r_Y(\varphi)$.

The map $X \to r_X$ transforms star-shaped figures into elements of a function space. Radius-vector functions of star-shaped figures are continuous in φ, consequently they can be embedded in the Banach space $C[0, 2\pi]$ of all continuous functions on $[0, 2\pi]$.

When the radius-vector function $r_X(\varphi)$ of a star-shaped figure X is known, some geometrical figure parameters can be obtained. Integrating $r_X(\varphi)$ yields perimeter $P(X)$, area $A(X)$, and mean radius-vector length $\bar{r}_X$:

$$P(X) = \int_0^{2\pi} \sqrt{r_X^2(\varphi) + r_X'^2(\varphi)}\, d\varphi,$$

$$A(X) = \frac{1}{2} \int_0^{2\pi} r_X^2(\varphi)\, d\varphi, \text{ and } \bar{r}_X = \frac{1}{2\pi} \int_0^{2\pi} r_X(\varphi)\, d\varphi.$$

A quantitative index of the differences between radius-vector functions of different figures may be obtained using the average squared deviation of the radius-vector function from a circle of equal area. This "*roughness coefficient*" is defined as:

$$R'_X = \frac{1}{2\pi} \int_0^{2\pi} r_X^2(\varphi)\, d\varphi - \left(\frac{1}{2\pi} \int_0^{2\pi} r_X(\varphi)\, d\varphi \right)^2.$$

2.3. Support Function

Support functions are frequently used to describe convex figures [41, 46]. For figure X the *support function* is defined as follows. Let g_φ be an oriented line passing through the origin O with the direction φ ($0 \leq \varphi \leq 2\pi$) and let $g_\varphi^\perp$ be the line orthogonal to g_φ with the property that figure X lies completely in that half-plane determined by $g_\varphi^\perp$ with $g_\varphi^\perp \cap X \neq \emptyset$, which is opposite to the direction of g_φ (Fig. 5(a)). The absolute value of the support function equals to the distance from O to $g_\varphi^\perp$ and the support function $s_X(\varphi)$ is negative if the figure lies behind $g_\varphi^\perp$ as seen from the origin. If O is an element of the figure, then $s_X(\varphi) \geq 0$ for all φ.

An equation to calculate the support function $s_X(\varphi)$ can be written using the *normal equation* of the line. Consider the closed contour of figure X in Euclidean space. Let the perimeter of the figure be L. Every point $(x_X(l), y_X(l))$ of the contour of X can thus be identified with a number l, $0 \leq l \leq L$, that runs through anti-clockwise. Then the support function $s_X(\varphi)$ can be calculated as

$$s_X(\varphi) = \max_{0 \leq l \leq L} \{x_X(l) \cos \varphi + y_X(l) \sin \varphi\}.$$

It is obvious that there exist different non-convex figures with the same support function (Fig. 5(b)). In contrast, convex figures are uniquely determined by their support functions. If $s_X(\varphi)$ is twice differentiable then figure X itself must be convex. An example of a convex figure and its support function is given in Fig. 6.

The support function $s_X(\varphi)$ of a convex figure X

1. in general, is not invariant under translation except for the case when O is an element of figure X;
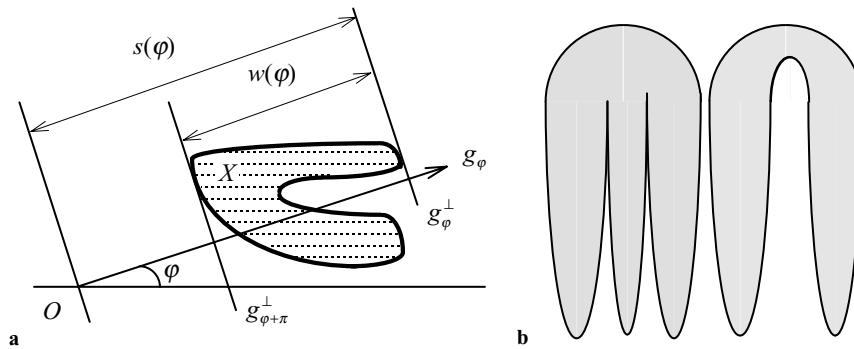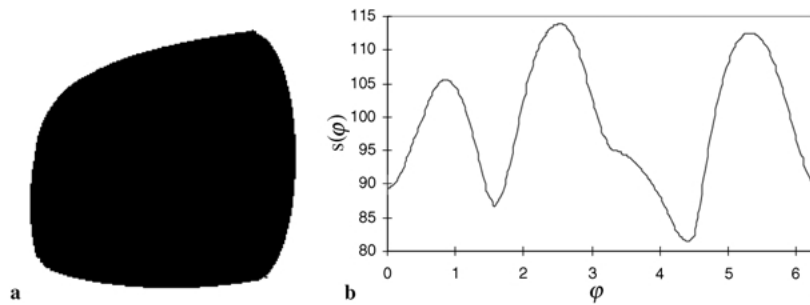

Figure 5.   (a) definition of the support function $s_X(\varphi)$ and the width function $w_X(\varphi)$ of figure X; (b) both figures have the same support function.

Figure 6. (a) convex figure X; (b) support function $s_X(\varphi)$ of figure X. The center of gravity of the figure was used as the origin to generate the support function.

2. depends on the changes of the size of the figure: $s_{\lambda X}(\varphi) = \lambda s_X(\varphi)$ where λX is figure X zoomed by a factor λ;

3. depends on the orientation of the figure: $s_X(\varphi) = s_Y(\varphi - \alpha)$ where Y is figure X rotated by an angle α;

4. is not invariant under reflection;

5. is periodic with the period 2π: $s_X(\varphi + 2\pi) = s_X(\varphi)$;

6. if a convex figure X is a subset of a convex figure Y ($X \subset Y$), then $s_X(\varphi) \leq s_Y(\varphi)$;

7. if a convex figure X is symmetric, then $s_X(\varphi) = s_X(\varphi + \pi)$.

The map $X \to s_X$ transforms convex figures into elements of a function space. Consequently, support functions of convex figures can be embedded in the Banach space $C[0, 2\pi]$ of all continuous functions on $[0, 2\pi]$.

If a convex figure X has a smooth boundary, then its support function $s_X(\varphi)$ determines the curvature. The curvature radius $\rho_X(\varphi)$ of the figure corresponding to φ is related to the support function $s_X(\varphi)$ as $\rho_X(\varphi) = s_X(\varphi) + s_X''(\varphi)$ where $0 \leq \varphi \leq 2\pi$. Having support

function $s_X(\varphi)$ of a convex figure X, its perimeter $P(X)$ and area $A(X)$ satisfy

$$P(X) = \int_0^{2\pi} s_X(\varphi) \, d\varphi \text{ and}$$

$$A(X) = \frac{1}{2} \int_0^{2\pi} s_X(\varphi)(s_X(\varphi) + s_X''(\varphi)) \, d\varphi.$$

2.4. Width Function

The so-called *width function* $w_X(\varphi)$ (Fig. 5(a)) is closely connected with the support function: $w_X(\varphi) = s_X(\varphi) + s_X(\varphi + \pi)$ where $0 \leq \varphi \leq \pi$ [46]. Physically $w_X(\varphi)$ is the breadth of the figure in the direction φ. For shape analysis the width function has the advantage that it is invariant with respect to translation: $w_{X+x}(\varphi) = w_X(\varphi)$. But rotation changes the width function. In general, the width function does not describe the form of a figure uniquely even if the figure is convex. An example of a figure and its width function is given in Fig. 7.

Having the width function $w_X(\varphi)$ of figure X, some contour parameters can be obtained. Thus, perimeter
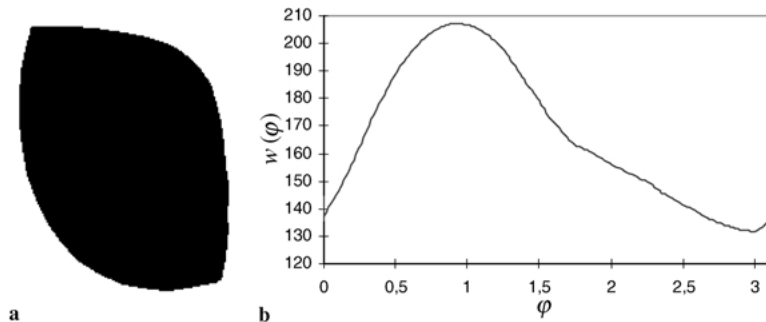

Figure 7. (a) figure X; (b) width function $w_X(\varphi)$ of figure X.

$P(X)$ of the figure can be yielded as

$$P(X) = \frac{1}{2} \int_0^{2\pi} w_X(\varphi)\, d\varphi,$$

however, the area is not uniquely determined by the width function.

2.5. Contour Parametric and Contour Complex Functions

Consider the closed contour of figure X in Euclidean space and let the perimeter of figure X be L. Every point $p_l(x_X(l), y_X(l))$ of the contour of X can thus be identified with a number l, with $0 \leq l \leq L$, running through anti-clockwise. A point moving along the contour in the anti-clock-wise direction generates a function which can be represented parametrically as $c_X(l) = (x_X(l), y_X(l))$. Contour parameterization in which the contour is parameterized by its arc length is called *natural parameterization*.

Consider the closed contour of figure X in polar coordinates. Every point p_l of the contour of X has polar coordinates $(d_X(l), \theta_X(l))$. A point moving along the contour in the anti-clockwise direction generates

a function which can be represented parametrically as $\tau_X(l) = (d_X(l), \theta_X(l))$.

Finally, consider the closed contour of figure X in the complex plane. Every point p_l of the contour of X has its complex coordinates $z_X(l) = x_X(l) + i y_X(l)$. A point moving along the contour in the anti-clockwise direction generates a complex function $z_X(l)$.

It is important to note that all three contour functions are identical. That is, when one contour function representation is known, the other two can be easily obtained:

$$z_X(l) = x_X(l) + i y_X(l),\; c_X(l) = (\operatorname{Re} z_X(l), \operatorname{Im} z_X(l)),$$
$$\tau_X(l) = (|z_X(l)|, \arg z_X(l)),\; c_X(l)$$
$$= (|d_X(l)| \cos \theta_X(l), |d_X(l)| \sin \theta_X(l)).$$

Examples of contour parametric functions are given in Fig. 8. The functions are not invariant under translation of the figure, are not invariant under changes of the size of the figure, depend on the orientation of X, are not invariant under reflection of the figure, and are periodic with the period L.

For shape analysis it is sometimes helpful to normalize these functions in such a way that the perimeter length is eliminated and the functions are defined on
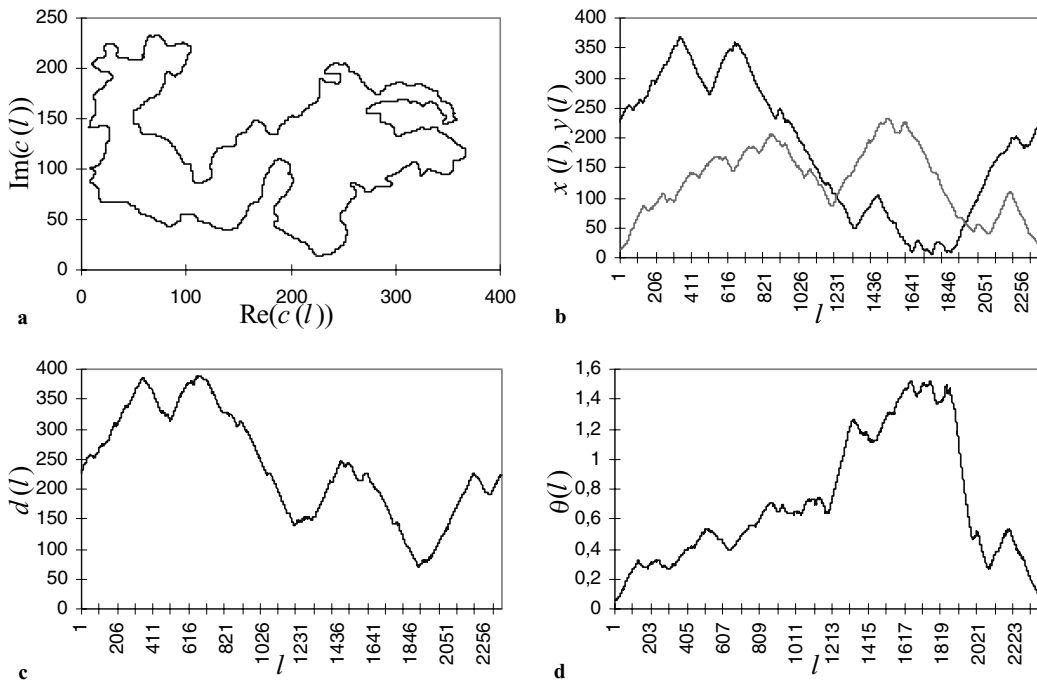

Figure 8. (a) complex function $z_X(l)$ of figure X; (b) parametric function $c_X(l) = (x_X(l), y_X(l))$ of figure X; (c, d) parametric function $\tau_X(l) = (d_X(l), \theta_X(l))$ of figure X.

$[0, 2\pi]$. This can be done in the following way [40]. The perimeter is normalized by defining $t = 2\pi l L^{-1}$ and the functions are normalized as $c_X^*(t) = c_X(tL(2\pi)^{-1})$, $\tau_X^*(t) = \tau_X(tL(2\pi)^{-1})$ and $z_X^*(t) = z_X(tL(2\pi)^{-1})$.

When one of these functions is known for figure X, some geometrical figure parameters can be calculated. Perimeter $P(X)$ of the contour is

$$P(X) = \int_0^L \sqrt{x_X'^2(l) + y_X'^2(l)}\, dl.$$

Oriented figure area $A(X)$ is given by the well-known differential geometry formula

$$A(X) = \frac{1}{2} \oint_{(C)} \left(x_X(l)\frac{dy_X(l)}{dl} - y_X(l)\frac{dx_X(l)}{dl} \right) dl$$

where $A(X)$ is positive or negative depending on where the figure is located when it is traced on the contour C- from the left or right side, respectively. Equations of the *tangent* and *normal* at a point $(x_X(l), y_X(l))$ of figure X are:

$$\frac{y - y_X(l)}{y'_X(l)} = \frac{x - x_X(l)}{x'_X(l)} \quad \text{and}$$
$$x_X'(l)(x - x_X(l)) + y_X'(l)(y - y_X(l)) = 0.$$

The *curvature* $\kappa_X(l)$ and *curvature radius* $\rho_X(l)$ at the point $(x_X(l), y_X(l))$ of the contour of X can be calculated as

$$\kappa_X(l) = \frac{x'_X(l)y''_X(l) - x''_X(l)y'_X(l)}{\left(x_X'^2(l) + y_X'^2(l)\right)^{3/2}} \quad \text{and}$$
$$\rho_X(l) = \frac{1}{|\kappa_X(l)|}.$$

Coordinates (x_k, y_k) *of* the *center of curvature* at the point $(x_X(l), y_X(l))$ of the contour of figure X are defined as

$$x_k = x_X(l) - \frac{y'_X(l)\left(x_X'^2(l) + y_X'^2(l)\right)}{x'_X(l)y''_X(l) - y'_X(l)x''_X(l)} \quad \text{and}$$
$$y_k = y_X(l) + \frac{x'_X(l)\left(x_X'^2(l) + y_X'^2(l)\right)}{x'_X(l)y''_X(l) - y'_X(l)x''_X(l)}$$

Contour parametric function $c_X(l)$ can be presented in a scaling function basis as [21]

$$c_X(l) = \sum_{k=-\infty}^{\infty} b_k \varphi(l - k) \quad \text{where}$$
$$\varphi(t) = \sum_k h(k)\varphi(2t - k)$$

In this representation, φ is called the scaling function and it satisfies the two-scale difference equation where $h(k)$ is the mask of the corresponding refinement filter; b_k denotes the sequence of vector coefficients. This description of $c_X(l)$ is equivalent to a periodized wavelet representation [8]. Also, a case of special interest is $\varphi = \beta^n$ where β^n is the casual B-spline of degree n.

2.6. Tangent-Angle Function

Often the tangent angle at different points of the contour is used for the description of a figure [16, 46]. It is assumed that the contour of figure X is piecewise-smooth so that a tangent may not exist at only a finite number of points.

Let the perimeter of figure X be L. Every point p_l of the contour of X can thus be identified with a number l, with $0 \le l \le L$, running through anti-clockwise. A pointer is placed at p_0 so that its zero position coincides with the tangent direction at p_0. If the pointer moves on the contour, then it changes its direction in such a way that it is always in the direction of the tangent, where its orientation is given by the direction of the movement. The angle given by the pointer direction at p_l is denoted $\phi_X(l)$ where $\phi_X(0) = 0$ and $\phi_X(L) = 2\pi$ (Fig. 9). The function $\phi_X(l)$ is called the *tangent-angle function*.

Sometimes it is helpful to normalize function $\phi_X(l)$ in such a way that the perimeter length is eliminated and the function is defined on $[0, 2\pi]$, like the radius-vector and support functions. In practice it can be done in the following way. The perimeter is normalized by defining $t = 2\pi l L^{-1}$ and $\phi_X(l)$ is normalized as $\phi_X^*(t) = \phi(Lt(2\pi)^{-1}) + t$ where $0 \le t \le 2\pi$ and $\phi_X^*(0) = \phi_X^*(2\pi) = 0$. Examples of a figure and its normalized tangent angle function are given in Fig. 10. The normalized tangent-angle function $\phi_X^*(t)$ of figure X

1. is invariant under translation: $\phi_{X+v}^*(t) = \phi_X^*(t)$ where $X + v$ is X translated by a vector v;
2. is invariant under changes of the size of the figure: $\phi_{\lambda X}^*(t) = \phi_X^*(t)$ where λX is figure X zoomed by a factor λ;
3. does not depend on the orientation of the figure;
4. is not invariant under reflection;
5. is periodic with the period 2π: $\phi_X^*(t + 2\pi) = \phi_X^*(t)$.

The map $X \to \phi_X^*$ transforms figures into elements of a function space, but the normalized tangent-direction functions of figures in general are not continuos.
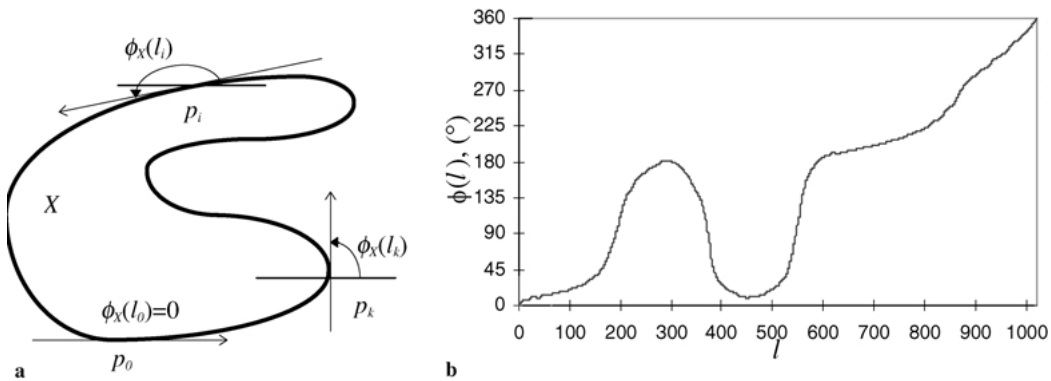
Figure 9.   (a, b) definition of the tangent-angle function $\phi_X(l)$ of figure X.
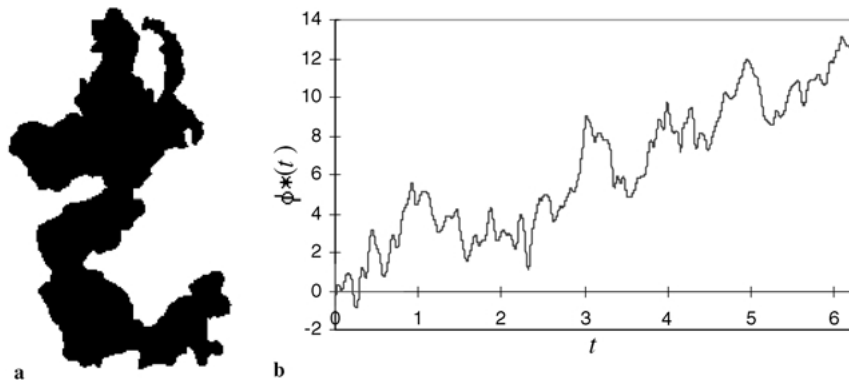

Figure 10.   (a) figure X; (b) the normalized tangent-angle function $\phi_X^*(t)$ of figure X.

Chain code [22] is an important discrete version of the tangent-angle function for the case of digital contours. The result of chain encoding is a direction from a point of the contour to its nearest neighbor point along the contour in the anti-clockwise direction as the function of the index of the contour point. Such function is a sequence of numbers $0, 1, \ldots, 7$ that correspond to $0°, 45°, 90°, \ldots, 315°$ angles.

2.7.   The Intrinsic Equation of the Contour

The *intrinsic equation* of the contour is defined to be the curvature as a function of the contour arc length [5, 6, 9, 14, 18, 20, 30, 43, 45, 51]. Such representation of the contour plays a key role in differential geometry. The importance of this function is immediately clear when looking at the *fundamental theorem* in the analysis of curves: *if two single-valued continuous functions are given, then there exists one and only one planar curve, determined but for its position on the plane, for which*

one of the given functions is the arc length (measured from an appropriate point on the curve) and other is the curvature.

Three different definitions of the curvature can be given:

(i)   orientation based continuous curvature:

$$\kappa_X(l) = \phi_X'(l);$$

(ii)   path based continuous curvature:

$$\kappa_X(l) = \frac{x_X'(l)y_X''(l) - x_X''(l)y_X'(l)}{\left(x_X'^2(l) + y_X'^2(l)\right)^{3/2}};$$

(iii)   osculating circle based continuous curvature:

$$\kappa_X(l) = \begin{cases} +\dfrac{1}{\rho_X(l)} & \text{if contour is locally convex} \\ -\dfrac{1}{\rho_X(l)} & \text{if contour is locally concave} \end{cases}$$
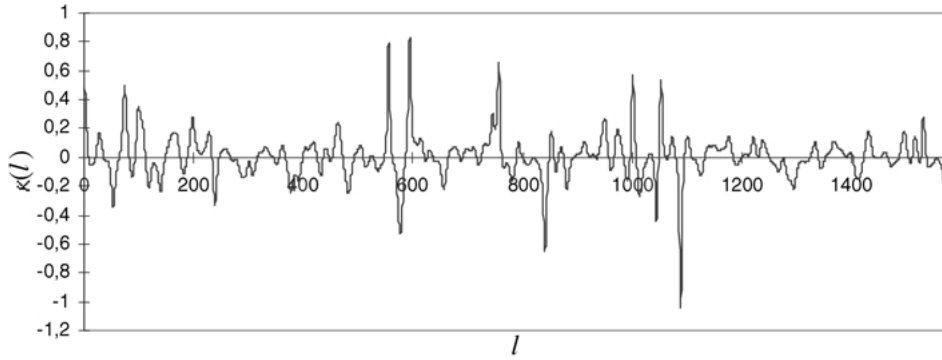
Figure 11.   Curvature function $\kappa_X(l)$ of figure X shown in Fig. 10(a).

The definitions are equivalent in the continuous case but not so in the discrete case. Different numerical methods of curvature estimation are based on either one of these definitions. An example of a curvature function is given in Fig. 11.

The curvature function has the same properties as those mentioned for the tangent-angle function. Some geometrical contour features are related to the contour curvature function $\kappa_X(l)$. Thus, the *corners* are locations on the contour where the curvature $\kappa_X(l)$ becomes unbounded. In practice, a corner is declared whenever $|\kappa_X(l)|$ assumes a large value.

Another attribute associated with the curvature is the *bending energy*:

$$E_X = \frac{1}{L} \int_0^L |\kappa_X(l)|^2 \, dl.$$

Also the definition of the *detrended function* $\hat{\theta}_X(l)$ of the contour is closely related to its curvature:

$$\hat{\theta}_X(l) = \int_o^l \kappa(p) \, dp - \frac{2\pi l}{L}.$$

2.8.   Algebraic Curve Model

An *algebraic curve* of the order n is defined as the zero set of polynomial p_n in two variables [47]:

$$p_n(x, y) = \sum_{0 \leq k, j, k+j \leq n} a_{kj} x^k y^j = \mathbf{Y}^{\mathrm{T}} \mathbf{A} = 0$$

The polynomial coefficients vector $\mathbf{A}$ consists of $\frac{1}{2}(n+1)(n+2)$ coefficients a_{kj} with $0 \leq k, j, k+j \leq n$ and vector $\mathbf{Y} = [1, x, y, x^2, xy, y^2, \ldots, y^n]^{\mathrm{T}}$. An

algebraic curve of degree 2 is a *conic*, degree 3 is a *cubic*, and so on.

A complex representation of an algebraic curve is also possible and it provides a simplified framework for analyzing rotation and translation. Using complex variables $z = x + iy$ and $\bar{z} = x - iy$ and binomial expansions for $(z + \bar{z})^k$ and $(z - \bar{z})^j$, $p_n(x, y)$ can be written as

$$p_n(z) = \sum_{0 \leq k, j, k+j \leq n} c_{kj} \bar{z}^k z^j = \bar{Z}^{\mathrm{T}} C = 0$$

where $C = (c_{kj})$ are complex linear combination of a_{kj} and Z is the vector of complex monomials.

The algebraic curve $p_n(x, y)$ of figure X is not invariant under translation, change of size, rotation, and reflection. However, translational dependence can be canceled by centering the polynomial at the origin of the coordinate system; rotational invariants can be obtained too.

2.9.   Parametric Cubic Curves

The contour parametric function $c_X(l)$ can be cut in finite segments. Each such curve segment s can be approximated by high-degree polynomial [15]

$$Q_s(l) = [x_s(l) \ y_s(l)] = \left[\sum_{k=0}^n b_{xk} l^k \ \sum_{k=0}^n b_{yk} l^k \right]$$

where b_{xk} and b_{yk} are polynomial coefficients and $x_s(l)$ and $y_s(l)$ refer to the contour parametric function $c_s(l)$ defined on segment s. Cubic polynomials $f(l) = b_{f0} + b_{f1} l + b_{f2} l^2 + b_{f3} l^3$ are most often used because of their properties, although higher-degree

polynomials can be used too. Each curve segment $Q_s(l)$ is defined by constraints on end points, tangent vectors, and continuity between curve segments. Depending on what constraints are used to define $Q_s(l)$, different types of curves can be obtained.

Cubic *Hermite curves* are defined by two end points, p_1, p_4, and two end point tangent vectors, r_1, r_4:

$$Q(l) = (2l^3 - 3l^2 + 1)p_1 + (-2l^3 + 3l^2)p_4$$
$$+ (l^3 - 2l^2 + l)r_1 + (l^3 - l^2)r_4$$

Consecutive Hermite cubics must share end points and tangent vectors with at least equal directions in order to continuously approximate a closed shape defined by its parametric function $c_X(l)$. Cubic *Bézier curves* are defined by two end points and two other points, p_2, p_3, that control the endpoint tangent vector:

$$Q(l) = (1 - l)^3 p_1 + 3l(1 - l)^2 p_2 + 3l^2(1 - l)p_3 + l^3 p_4$$

Two consecutive Bézier curve segments with a common end point continuously approximate the shape when the common end point and its immediate 2 neighbor points are distinct and collinear. Uniform cubic *B-splines* approximate a series of $m + 1$ control points $p_0, \ldots, p_m, m \geq 3$, with a curve consisting of $m - 2$ cubic polynomial curve segments $Q_3, \ldots, Q_m$. Thus, for $m = 3$, Q_3 is defined by $p_0, \ldots, p_3$, Q_4 is defined by $p_1, \ldots, p_4$, and so on:

$$Q_i(l - l_i) = \frac{(1 - l)^3}{6} p_{i-3} + \frac{3l^3 - 6l^2 + 4}{6} p_{i-2}$$
$$+ \frac{-3l^3 + 3l^2 + 3l + 1}{6} p_{i-1} + \frac{l^3}{6} p_i$$

Joint points l_i between Q_i and Q_{i+1} are called *knots* and Q_i and Q_{i+1} are continuous at l_i. In the case of uniform B-splines, knots are equally spaced on l.

Uniformly shaped *β-splines* differ from B-splines by requiring 2 additional parameters, β_1 and β_2, to provide further control over shape. The first parameter is called the *bias* parameter and it influences how the tangent vector affects the spline, the second parameter is called *tension* parameter and as it increases the spline is pulled closer to the lines connecting the control points. Non-uniform B-splines, rational cubic polynomials, and Overhauser splines [15] are just a few examples of other parametric cubic curves used to approximate the shape.

3.   Analysis of Contour Functions

Although some shape properties can be computed directly from the shape functions, it is more advantageous to further analyze these functions so that a more meaningful and compact shape description is obtained. Several practical contour function analysis techniques are described below. Again, as with the shape functions, not all such techniques are included and some techniques are covered only briefly.

3.1.   Invariant Contour Function Parameters

Some simple quantities of contour functions can be determined [46]. Thus, the *mean value* of a contour function $f(x)$ is given by

$$\bar{f} = \frac{1}{2\pi} \int_0^{2\pi} f(x)\, dx \approx \frac{1}{N} \sum_{i=1}^{N} f(x_i).$$

The mean value $\bar{f}$ of a contour function $f(x)$ is a size parameter except in the case of the tangent-vector, contour curvature and contour parametric functions. In the latter case, it reveals the center of gravity of the contour.

Variance of a contour function $f(x)$ is given by

$$\sigma^2(f) = \frac{1}{2\pi} \int_0^{2\pi} [f(x) - \bar{f}]^2\, dx$$
$$\approx \frac{1}{N} \sum_{i=1}^{N} (f(x_i) - \bar{f})^2.$$

The variance $\sigma^2(f)$ of a contour function $f(x)$ is a size, shape and roundness characteristic.

Variance of the derivative of a contour function $f(x)$ is given by

$$\sigma^2(f') = \frac{1}{2\pi} \int_0^{2\pi} f'^2(x)\, dx$$
$$\approx \frac{1}{N} \sum_{i=1}^{N} \left(\frac{f(x_{i-2}) - 8f(x_{i-1}) + 8f(x_{i+1}) - f(x_{i+2})}{12\Delta} \right)^2$$

where $\Delta = 2\pi N^{-1}$, $x_{-1} = x_{N-1}, x_0 = x_N, x_{N+1} = x_1, x_{N+2} = x_2$. The variance $\sigma^2(f')$ of the derivative describes local properties such as roundness and texture variations.

The covariance function of a contour function $f(x)$ is given by

$$\chi_f(\varphi) = \frac{1}{2\pi} \int_0^{2\pi} [f(x) - \bar{f}][f(x + \varphi) - \bar{f}] \, dx,$$

$$\chi_f(k\Delta) = \frac{1}{N} \sum_{i=1}^{N} [f(x_i) - \bar{f}][f(x_{i+k}) - \bar{f}]$$

where $0 \leq \varphi \leq 2\pi$, $f(2\pi + x) = f(x)$, $x_{N+k} = x_k$. Covariance $\chi_f(\varphi)$ describes some aspects of local and global form fluctuations. The normalized function $\chi_f(\varphi)\chi_f^{-1}(0)$ characterizes the shape of the figure.

Quantities $\bar{f}$ and $\sigma^2(f)$ can be interpreted as mean and variance corresponding to a distribution function $F_f(x)$, defined as

$$F_f(x) = \frac{1}{2\pi}\mathbf{L}(\{\varphi : f(\varphi) \leq 0; 0 \leq \varphi \leq 2\pi\}), x \geq 0$$

where $\mathbf{L}$ denotes the Lebesgue measure of R^1 which is the length for a regular set in R^1. The distribution function $F_f(x)$ of a contour function $f(x)$ is a size, shape and roundness characteristic.

3.2. Line Moments and Invariants

A useful and practical set of shape descriptors is based on the theory of moments, which for the case of the figure contour can be introduced as follows [26, 27]. Consider the parametric representation $c_X(l)$ of the contour C of figure X. *Line moments* along the contour are given by

$$m_{p,q}^{(1)} = \oint_{(C)} x_X^p(l)y_X^q(l)\delta(l) \, dl$$

where $\delta(l)$ is a linear density of the contour, which for simplicity can be taken as 1. The number $p + q$ is called the *order* of the moment. Calculation of the linear moments for discretized curves can be performed as

$$m_{p,q}^{(1)} \approx \sum_{i=1}^{N} (x_X(l_i))^p (y_X(l_i))^q$$

where N is the number of available points of the contour C. This formula is different when only an approximation of the contour by a polygon is available. If the contour is approximated by an n-side polygon with vertexes (x_i, y_i) where $i = 1, 2, \ldots n$, each line segment

u_i can be parameterized by $y = a_i x + y_i - a_i x_i$ where $x_i \leq x \leq x_{i+1}$ and $a_i = (y_{i+1} - y_i)/(x_{i+1} - x_i)$ is the slope of the segment u_i. If the segment is vertical, the alternative parameterization should be used: $x = x_i$ where $y_i \leq y \leq y_{i+1}$. Then the following formula can be used to calculate the linear moments:

$$m_{p,q}^{(1)} \approx \sum_{i=1}^{n} \left[\begin{cases} \sqrt{1+a_i^2} \sum_{k=0}^{q} \left\{ C_k^q a_i^k (y_i - a_i x_i)^{q-k} \right. \\ \left. \times \frac{x_{i+1}^{p+k+1} - x_i^{p+k+1}}{p+k+1} \right\} \\ \qquad\qquad\qquad \text{if } u_i \text{ is not vertical} \\ x_i^p \frac{y_{i+1}^{q+1} - y_i^{q+1}}{q+1} \quad \text{if } u_i \text{ is vertical} \end{cases} \right]$$

where C_k^q are binomial coefficients.

Line moments are not invariant under the main geometrical transformations such as translation, rotation, scale change and reflection. However *central moments* are invariant under translation. To obtain them, the center of gravity of the contour C should be calculated which, actually, can be expressed through the zero- and first-order line moments:

$$\bar{x} = m_{1,0}^{(1)}/m_{0,0}^{(1)} \quad \text{and} \quad \bar{y} = m_{0,1}^{(1)}/m_{0,0}^{(1)}.$$

Then central moments are just

$$\mu_{p,q}^{(1)} = \oint_{(C)} (x_X(l) - \bar{x})^p (y_X(l) - \bar{y})^q \delta(l) \, dl.$$

Central moments up to the third order are also given by the following relations:

$$\mu_{0,0}^{(1)} = m_{0,0}^{(1)}, \mu_{1,0}^{(1)} = \mu_{0,1}^{(1)} = 0, \mu_{2,0}^{(1)} = m_{2,0}^{(1)} - m_{0,0}^{(1)}\bar{x}^2,$$
$$\mu_{1,1}^{(1)} = m_{1,1}^{(1)} - m_{0,0}^{(1)}\bar{x}\bar{y}, \mu_{0,2}^{(1)} = m_{0,2}^{(1)} - m_{0,0}^{(1)}\bar{y}^2,$$
$$\mu_{3,0}^{(1)} = m_{3,0}^{(1)} - 3m_{2,0}^{(1)}\bar{x} + 2m_{0,0}^{(1)}\bar{x}^3,$$
$$\mu_{2,1}^{(1)} = m_{2,1}^{(1)} - m_{2,0}^{(1)}\bar{y} - 2m_{1,1}^{(1)}\bar{x} + 2m_{0,0}^{(1)}\bar{x}^2\bar{y},$$
$$\mu_{1,2}^{(1)} = m_{1,2}^{(1)} - m_{0,2}^{(1)}\bar{x} - 2m_{1,1}^{(1)}\bar{y} + 2m_{0,0}^{(1)}\bar{x}\bar{y}^2 \quad \text{and}$$
$$\mu_{0,3}^{(1)} = m_{0,3}^{(1)} - 3m_{0,2}^{(1)}\bar{y} + 2m_{0,0}^{(1)}\bar{y}^3.$$

Scale-invariant line moments can be obtained by normalizing the contour by its length:

$$\eta_{p,q}^{(1)} = \mu_{p,q}^{(1)} \left(\mu_{0,0}^{(1)}\right)^{-(p+q+1)}.$$

Under rotation and reflection the moment-generation function will change. However, via the theory of algebraic invariants it is possible to find certain polynomials of the central line moments that remain unchanged under rotation and reflection. Some moment invariants are:

(i) for first-order moments: $\mu_{1,0}^{(1)} = \mu_{0,1}^{(1)} = 0$ are always invariant;

(ii) for second-order moments the invariants are:

$$\phi_1^{(1)} = \mu_{2,0}^{(1)} + \mu_{0,2}^{(1)} \quad \text{and}$$
$$\phi_2^{(1)} = \left(\mu_{2,0}^{(1)} - \mu_{0,2}^{(1)}\right)^2 + 4\left(\mu_{1,1}^{(1)}\right)^2;$$

(iii) for third-order moments the invariants are:

$$\phi_5^{(1)} = \left(\mu_{3,0}^{(1)} - 3\mu_{1,2}^{(1)}\right)\left(\mu_{3,0}^{(1)} + \mu_{1,2}^{(1)}\right)\left(\left(\mu_{3,0}^{(1)} + \mu_{1,2}^{(1)}\right)^2 \right.$$
$$- 3\left(\mu_{2,1}^{(1)} + \mu_{0,3}^{(1)}\right)^2\right) + \left(\mu_{0,3}^{(1)} - 3\mu_{2,1}^{(1)}\right)$$
$$\times \left(\mu_{0,3}^{(1)} + \mu_{2,1}^{(1)}\right)\left(\left(\mu_{0,3}^{(1)} + \mu_{2,1}^{(1)}\right)^2 \right.$$
$$- 3\left(\mu_{1,2}^{(1)} + \mu_{3,0}^{(1)}\right)^2\right),$$
$$\phi_3^{(1)} = \left(\mu_{3,0}^{(1)} - 3\mu_{1,2}^{(1)}\right)^2 + \left(\mu_{0,3}^{(1)} - 3\mu_{2,1}^{(1)}\right)^2,$$
$$\phi_4^{(1)} = \left(\mu_{3,0}^{(1)} + \mu_{1,2}^{(1)}\right)^2 + \left(\mu_{0,3}^{(1)} + \mu_{2,1}^{(1)}\right)^2 \quad \text{and}$$
$$\phi_6^{(1)} = \left(\mu_{2,0}^{(1)} - \mu_{0,2}^{(1)}\right)\left(\left(\mu_{3,0}^{(1)} + \mu_{1,2}^{(1)}\right)^2 \right.$$
$$- \left(\mu_{2,1}^{(1)} + \mu_{0,3}^{(1)}\right)^2\right)$$
$$+ 4\mu_{1,1}^{(1)}\left(\mu_{0,3}^{(1)} + \mu_{1,2}^{(1)}\right)\left(\mu_{0,3}^{(1)} + \mu_{2,1}^{(1)}\right);$$

(iv) it has been shown [22] that for Nth-order moments where $N \geq 3$, there are $N + 1$ absolute invariants, which remain unchanged under both reflection and rotation. A number of other invariants can be found that remain unchanged under rotation but change sign under reflection.

The relationship between invariant moments becomes more complicated for higher-order moments. However, moment invariants can be expressed more conveniently in terms of what are called *Zernike moments*. These moments are defined as the projections of a function of two variables on a class of Zernike polynomials.

Being invariant under linear coordinate transformations, the moment invariants are useful features in pattern recognition. Using N moments, a contour can be represented as a point in an N-dimensional vector space and the pattern recognition problem thus is converted into a standard decision theory problem, for which several approaches are available.

Several figure parameters are based on moments. The figure's *orientation* θ is the angle between the major axis of the figure and the x axis of the coordinate system in which the figure is considered:

$$\theta = \frac{1}{2}\arctan\left(\frac{2\mu_{1,1}^{(1)}}{\mu_{2,0}^{(1)} - \mu_{0,2}^{(1)}}\right).$$

Once θ is known, the *bounding rectangle* of the figure can be determined. The bounding rectangle is the smallest rectangle enclosing the object that is also aligned with its orientation. Its sides can be calculated as

$$h = \max\{x_X(l)\cos\theta + y_X(l)\sin\theta\}$$
$$- \min\{x_X(l)\cos\theta + y_X(l)\sin\theta\}$$
$$w = \max\{-x_X(l)\sin\theta + y_X(l)\cos\theta\}$$
$$- \min\{-x_X(l)\sin\theta + y_X(l)\cos\theta\}$$

where $0 \leq l \leq L$. The *best-fit ellipse* of the figure can be also expressed in terms of the line moments. The best-fit ellipse is the ellipse whose second-order moments are equal to the second-order moments of the figure. Let a and b denote the length of semi-major and semi-minor axes of the best-fit ellipse. Then

$$a = \sqrt[4]{\frac{4}{\pi}}\sqrt[8]{\frac{\left(\mu(\theta)_{2,0}^{(1)}\right)^3}{\mu(\theta)_{0,2}^{(1)}}} \quad \text{and} \quad b = \sqrt[4]{\frac{4}{\pi}}\sqrt[8]{\frac{\left(\mu(\theta)_{0,2}^{(1)}\right)^3}{\mu(\theta)_{2,0}^{(1)}}}$$

where

$$\mu(\theta)_{0,2}^{(1)} \quad \text{and} \quad \mu(\theta)_{2,0}^{(1)}$$

are the second-order line moments of the contour C^* of figure X^*, which is obtained by rotating figure X by the angle $-\theta$.

The figure's *eccentricity* ε can be measured as:

$$\varepsilon = \sqrt{\frac{\mu_{0,2}^{(1)}\cos^2\theta + \mu_{2,0}^{(1)}\sin^2\theta - \mu_{1,1}^{(1)}\sin 2\theta}{\mu_{0,2}^{(1)}\sin^2\theta + \mu_{2,0}^{(1)}\cos^2\theta + \mu_{1,1}^{(1)}\cos 2\theta}}$$
$$= \frac{\left(\mu_{2,0}^{(1)} - \mu_{0,2}^{(1)}\right)^2 + 4\mu_{1,1}^{(1)}}{A(X)}.$$

Finally the figure's contour *spread* S can be calculated in terms of central moments as

$$S = \mu_{0,2}^{(1)} + \mu_{2,0}^{(1)}.$$

One of the advantages of line moments for shape analysis is that neither the existence of an area nor a closed contour is required. The line moments can be calculated for an arbitrary collection of contour fragments.

3.3. Fourier Transform

The Fourier transform is one of the most frequently used methods in shape analysis [2–4, 11–13, 17, 22, 24, 31, 32, 34, 42, 46, 48, 50]. Consider a periodic piecewise continuous and differentiable function $f(x)$ defined on $[0, 2\pi]$, which can be one of the contour functions described above. Such function can be approximated by a *Fourier series*:

$$f(x) = \frac{a_0}{2} + \sum_{k=1}^{\infty} (a_k \cos kx + b_k \sin kx)$$

where the *Fourier coefficients* are

$$a_k = \frac{1}{\pi} \int_{-\pi}^{\pi} f(x) \cos kx \, dx \quad \text{and}$$

$$b_k = \frac{1}{\pi} \int_{-\pi}^{\pi} f(x) \sin kx \, dx.$$

The Fourier series can be also written as

$$f(x) = \frac{a_0}{2} + \sum_{k=1}^{\infty} A_k \sin(kx + \varphi_k)$$

where $A_k = \sqrt{a_k^2 + b_k^2}$ and $\tan \varphi_k = a_k/b_k$, or in the complex form as

$$f(x) = \sum_{k=-\infty}^{\infty} c_k e^{ikx}$$

where

$$c_k = \frac{1}{2\pi}$$

$$\times \int_{-\pi}^{\pi} f(x) e^{-ikx} dx = \begin{cases} \dfrac{a_0}{2}, & \text{if } k = 0 \\ \dfrac{1}{2}(a_k - ib_k), & \text{if } k > 0 \\ \dfrac{1}{2}(a_{-k} + ib_{-k}), & \text{if } k < 0 \end{cases}$$

Each term of the Fourier series is called *harmonic* and A_k is the *harmonic amplitude*. The sequence $\{A_k\}$ is called the *amplitude spectrum*.

Some general properties of Fourier series expansion and Fourier coefficients are given below.

1. Coefficient a_0 equals to the mean value of $f(x)$.
2. Fourier coefficients depend in different ways on the shape of the figure: a_k, b_k and A_k for small k tend to describe the global characteristics, while coefficients for large k describe roughness;
3. Symmetry properties of the figure are reflected by Fourier coefficients. That is, if the function $f(x)$ has a smaller period than 2π, namely $2\pi/l$, where $l \in \mathbb{N}$ and $l > 1$, then if a_0 is excluded, only the coefficients a_k and b_k with $k = lm$ where $m = 1, 2, \ldots$ differ from zero.
4. The operation that assigns to function $f(x)$ its Fourier coefficients a_k and b_k is linear. That is, let $f(x)$ be given in the form $f(x) = \sum_{i=1}^{m} \gamma_i f_i(x)$ and let $a_k^{(i)}$ and $b_k^{(i)}$ be Fourier coefficients of functions $f_i(x)$, then Fourier coefficients of $f(x)$ can be written as

$$a_k = \sum_{i=1}^{m} \gamma_i a_k^{(i)} \quad \text{and} \quad b_k = \sum_{i=1}^{m} \gamma_i b_k^{(i)}.$$

5. Several geometrical transformations of the contour of a figure are related to simple operations on the corresponding Fourier coefficients. If a translation of the contour has an influence on the contour function (e.g., the contour complex function) then the new Fourier coefficients remain the same except for $k = 0$. Shrinking or expanding the contour by a factor α results in scaled Fourier coefficients, $c_k' = \alpha c_k$ where c_k and c_k' are Fourier coefficients of the original and scaled contours, respectively. Changing the starting point in tracing the contour results in a modulation of the coefficients, $c_k' = c_k e^{-ikx_0}$ where x_0 is the new starting point. Rotation of the contour by an angle θ_0 causes a constant phase shift of θ_0 in Fourier coefficients, $c_k' = c_k e^{i\theta_0}$; reflection of the contour about a straight line $Ax + By + C = 0$ gives the new contour for which

$$c_k' = c_{-k}^* \frac{-(A + iB)^2}{A^2 + B^2} + 2\delta_k \frac{-(A + iB)C}{A^2 + B^2}.$$

6. The A_k (for all k) and $|c_k|$ (for all k except $k = 0$) are invariant with respect to shift of the starting point (variable x), rotation and reflection of the contour. Features $c_k/|c_1|$, a_k/A_0, b_k/A_0 are invariant to scaling. Finally A_k/A_0 and $|c_k|/|c_1|$ are invariant to all
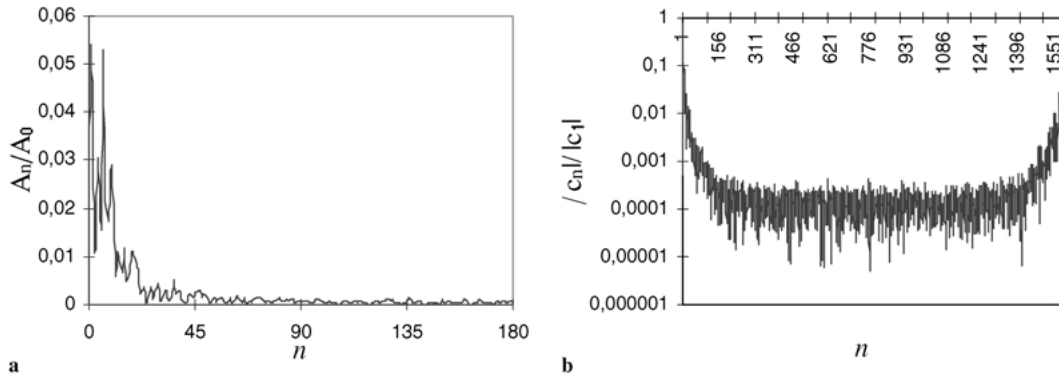
Figure 12.   (a) normalized amplitude spectrum $\{A_n/A_0\}$ for the radius-vector function shown in Fig. 4(b); (b) normalized amplitude spectrum $\{|c_n|/|c_1|\}$ (for all n except $n = 0$) for the contour complex function shown in Fig. 8(a).

above mentioned geometrical transformations. Examples of $\{A_k/A_0\}$ and $\{|c_k|/|c_1|\}$ for different contour functions are given in Fig. 12.

7. As in the theory of stochastic processes, there is a close connection between contour covariance function $\chi_f(\varphi)$ and the Fourier coefficients:

$$\chi_f(\varphi) = \frac{1}{2} \sum_{k=1}^{\infty} A_k^2 \cos k\varphi \quad \text{and}$$

$$A_k^2 = \frac{2}{\pi} \int_0^{2\pi} \chi_f(\varphi) \cos k\varphi \, d\varphi.$$

Often it is enough to consider only the A_k/A_0 ($k = 1, 2, \ldots$) coefficients and usually all necessary shape information is accumulated only in the very few first coefficients. Some shape parameters can be derived as shown below.

When the contour of a figure is described by the radius-vector function $r_X(\varphi)$, the following structure, size and shape terms are often used. The parameters for *global structure* and for *roughness* are

$$G_{n_1} = \sum_{n=1}^{n_1} A_n^2 \quad \text{and} \quad R_{n_2,n_3} = \sum_{n=n_2}^{n_3} A_n^2$$

where n_1, n_2 and n_3 are suitable natural numbers chosen with the figures to be analyzed in mind. The *size term* is

$$R_0 = \sqrt{a_0^2 + \frac{1}{2} \sum_{n=1}^{[(N+1)/2]-1} \left(a_n^2 + b_n^2\right)}$$

$$= \sqrt{A_0^2 + \frac{1}{2} \sum_{n=1}^{[(N+1)/2]-1} A_n^2}$$

where R_0 is called the *equivalent radius* and is the radius of a circle having the same area as that of the figure. In fact, the area of the figure may be stated in terms of Fourier coefficients as $A(X) = \pi R_0^2$.

The *shape terms* are

$$L_0 = \frac{a_0}{R_0} = \frac{A_0}{R_0}, \; L_1(n) = 0, \; L_2(n)$$

$$= \frac{(a_n^2 + b_n^2)}{2R_0^2} = \frac{A_n^2}{2R_0^2} \quad \text{and}$$

$$L_3(m, n) = \frac{3}{4R_0^3}(a_m a_n a_{n+m} - b_m b_n b_{n+m}$$
$$+ a_m b_n b_{n+m} + b_m a_n b_{n+m})$$
$$= \frac{3}{4R_0^3}(A_m A_n A_{n+m} \cos(\varphi_{n+m} - \varphi_m - \varphi_n))$$

where $n = 0, 1, \ldots, [(N + 1)/2] - 1$ and $n + m = 2, 3, \ldots, [(N + 1)/2] - 1$. The shape term L_0 is the size normalized mean radius of the figure radial distribution, however the interpretation of other shape terms is not so simple.

The quantity

$$L_2(n) \bigg/ \sum_{j=1}^{[(N+1)/2]-1} L_2(j)$$

can be considered as a measure of the proportion of the radial variability of the figure that can be attributed to the nth harmonic. Partial sum

$$\sum_{j=1}^{k} L_2(j)$$

can be used to describe how well the first k harmonics fit the observed radii. The size and shape terms are

directly related to the mean μ_0, first μ_1, second μ_2 and third μ_3 moments about the mean of the figure's radial distribution:

$$\mu_0 = L_0 R_0 = a_0, \mu_1 = R_0 \sum_{n=1}^{[(N+1)/2]-1} L_1(n) = 0,$$

$$\mu_2 = R_0^2 \sum_{n=1}^{[(N+1)/2]-1} L_2(n) \quad \text{and}$$

$$\mu_3 = R_0^3 \sum_{m=1}^{[(N+1)/2]-1} \sum_{n=1}^{[(N+1)/2]-1} L_3(m, n).$$

A quantitative index of differences between different amplitude spectra may be obtained by determining the average squared deviation of the radius-vector function from a circle of equal area. This "*roughness coefficient*" can be calculated as the square root of one-half the sum of the squared Fourier coefficients:

$$R' = \sqrt{\frac{1}{2} \sum_{n=1}^{[(N+1)/2]-1} \left(a_n^2 + b_n^2\right)} = \sqrt{\frac{1}{2} \sum_{n=1}^{[(N+1)/2]-1} A_n^2}.$$

Sometimes it is also convenient to consider a modified roughness coefficients spanning a selected range of harmonics rather than all of them:

$$R'_{n1,n2} = \sqrt{\frac{1}{2} \sum_{n=n_1}^{n_2} A_n^2}.$$

When the polar parametric function $\tau_X^*(t) = (d_X^*(t), \theta_X^*(t))$ is used, the following analysis can be done [4]. Fourier series expansions are used to represent $d_X^*(t)$ and $\theta_X^{*'}(l)$. The equivalent radius is then defined as

$$R_0^2 = \frac{1}{2\pi} \int_0^{2\pi} (d^*(t))^2 \theta^{*'}(t) \, dt.$$

The shape terms L_0, $L_2(n)$ and $L_3(m, n)$ for the $d_X^*(t)$ and $\theta_X^{*'}(l)$ expansions are defined in a similar way as described for the radius-vector function. For the case of the contour complex function $c_X^*(t)$ the useful information is accumulated in $|c_k|/|c_1|$ [22, 24, 48, 50]. Coefficient c_0 usually is not used because it reflects the contour position.

3.4. Other Series Expansions

There is a number of other series expansions [7, 22] that can be useful in shape analysis. Before introducing them, some general ideas of function series expansions are given. For continuous functions, orthogonal series expansions provide series coefficients which can be used for any further processing or analysis of the functions. For a one-dimensional function $f(x_r)$ given at N equally spaced points x_r, a unitary transformation is written as

$$u_n = \sum_{r=0}^{N-1} f(x_r) a_{r,n}^* \quad \text{where } f(x_r) = \sum_{n=0}^{N-1} u_n a_{r,n}.$$

This can be also written in a matrix form as $\mathbf{u} = \mathbf{A}\mathbf{f}$ where $\mathbf{A}^{-1} = \mathbf{A}^{*\mathbf{T}}$. This gives $\mathbf{f} = \mathbf{A}^{*\mathbf{T}}\mathbf{u}$ where the columns of $\mathbf{A}^{*\mathbf{T}}$, that is, the vectors $\mathbf{a}_r^* = \{a_{r,n}^*, 0 \leq n \leq N-1\}^{\mathbf{T}}$ are called the *basis vectors* of $\mathbf{A}$. The series coefficients u_n give a representation of function $f(x_r)$.

The *one-dimensional discrete cosine series expansion* of function $f(x_r)$ given at N equally spaced points x_r, is defined as

$$f(x_r) = \sum_{n=0}^{N-1} \alpha_n u_n \cos \frac{\pi(2n+1)r}{2N}$$

where $\alpha_n = \sqrt{2/N}$, $\alpha_0 = \sqrt{1/N}$ and

$$u_n = \alpha_n \sum_{r=0}^{N-1} f(x_r) \cos \frac{\pi(2n+1)r}{2N}.$$

The *one-dimensional discrete sine series expansion* of function $f(x_r)$ given at N equally spaced points $x_r (x_r = 2\pi r/N)$, is defined as

$$f(x_r) = \sqrt{\frac{2}{N+1}} \sum_{n=0}^{N-1} u_n \sin \frac{\pi(r+1)(n+1)}{N+1}$$

where

$$u_n = \sqrt{\frac{2}{N+1}} \sum_{r=0}^{N-1} f(x_r) \sin \frac{\pi(r+1)(n+1)}{N+1}.$$

The *one-dimensional discrete Walsh-Hadamard series expansion* of function $f(x_r)$ given at $N(N = 2^n)$

equally spaced points x_r, is defined as

$$f(x_r) = \frac{1}{\sqrt{N}} \sum_{m=0}^{N-1} u_m (-1)^{b(r,m)}$$

where

$$b(r,m) = \sum_{i=0}^{n-1} r_i m_i \quad (r_i, m_i = 0, 1)$$

and $\{r_i\}$, $\{m_i\}$ are the binary representations of r and m, that is

$$r = r_0 + 2r_1 + \cdots + 2^{n-1}r_{n-1} \quad \text{and}$$
$$m = m_0 + 2m_1 + \cdots + 2^{n-1}m_{n-1}.$$

The Walsh-Hadamard coefficients are computed as

$$u_m = \frac{1}{\sqrt{N}} \sum_{r=0}^{N-1} f(x_r)(-1)^{b(r,m)}.$$

The *one-dimensional discrete Haar series expansion* of function $f(x_r)$ given at $N(N = 2^n)$ equally spaced points x_r, is presented as follows. The *Haar functions* $h_{p,q}(x)$ are defined on a continuous interval, $x \in [0, 1]$, as

$$h_{0,0}(x) = \frac{1}{\sqrt{N}} \quad \text{and} \quad h_{p,q}(x)$$

$$= \frac{1}{\sqrt{N}} \begin{cases} 2^{p/2}, & \dfrac{q-1}{2^p} \leq x < \dfrac{q-1/2}{2^p} \\ -2^{p/2}, & \dfrac{q-1/2}{2^p} \leq x < \dfrac{q}{2^p} \\ 0, & \text{otherwise} \end{cases}.$$

The Haar transform is obtained by re-scaling x_r in such a way that $x'_r \in [0, 1]$, where $x'_r = g(x_r)$, and applying the matrix form of a unitary transform for $f(x'_r)$ and $h_{p,q}(x)$.

The *one-dimensional Gabor series expansion* of function $f(x)$ is defined based on the short-time Fourier transform:

$$u_{\varpi,\tau} = \int_{-\infty}^{\infty} g^*(t - \tau)u_t e^{-i2\pi\omega t}\, dt$$
$$= e^{-i2\pi\omega t} \int_{-\infty}^{\infty} \hat{g}^*(\nu - \varpi)\hat{u}_\nu e^{i2\pi\nu\tau}\, d\nu$$

where $\hat{u}_\nu$ and $\hat{g}$ denote the Fourier transforms of u_t and g, respectively, $*$ denotes the complex conjugate and the window is a Gaussian:

$$\hat{g}(\mu) = \frac{1}{\sigma\sqrt{2\pi}} e^{\frac{-\mu^2}{2\sigma^2}}.$$

Some other series expansions of the contour functions are reported in the literature including KL, Slant, sinusoidal, singular value decomposition series expansions [22], etc. However, their use in shape analysis is limited and therefore they are not described here.

One common way for analyzing series coefficients is through the identification and characterization of a few maximal coefficients. Another possible method of analysis is based on the idea that the same series coefficients for the same contour functions of different figures mean the same things and, therefore, can be compared. For the Gabor series expansion two other methods can be employed. The response of the transform for different parameters ω and τ can be used for the analysis. Also the projection of the response onto box axes generates images which can reveal essential features of the analyzed contour functions.

3.5. Shape Curvature Scale Space Image

A curvature scale space representation is a multi-scale organization of the invariant geometrical features such as the curvature zero-crossing points of a planar curve [33, 36–38, 43]. To compute it, contour parametric function $c_X(l)$ and contour curvature function $\kappa_X(l)$ are used. The *evolved* version of the contour C is defined as $C_\sigma = (X(l, \sigma), Y(l, \sigma))$ where $X(l, \sigma) = x(l) \otimes g(l, \sigma)$, $Y(l, \sigma) = y(l) \otimes g(l, \sigma)$, $\otimes$ is the convolution operator and $g(l, \sigma)$ denotes a one-dimensional Gaussian kernel of width σ:

$$g(l, \sigma) = \frac{1}{\sigma\sqrt{2\pi}} e^{\frac{-l^2}{2\sigma^2}}.$$

The convolution is defined as

$$F(l, \sigma) = f(l) \otimes g(l, \sigma) = \int_{-\infty}^{\infty} f(s) \frac{1}{\sigma\sqrt{2\pi}} e^{\frac{-(l-s)^2}{2\sigma^2}}\, ds$$
$$\approx \sum_{s=-3\sigma}^{3\sigma} f(l+s) \frac{1}{\sigma\sqrt{2\pi}} e^{\frac{-(l-s)^2}{2\sigma^2}}.$$

Then the curvature function $\kappa(l)$ for the evolved contour C_σ is calculated as

$$\kappa(l, \sigma) = \frac{X'(l, \sigma)Y''(l, \sigma) - X''(l, \sigma)Y'(l, \sigma)}{(X'^2(l, \sigma) + Y'^2(l, \sigma))^{3/2}}.$$

The process of generation of the ordered sequence of evolved contours from a contour C is called the *evolution* of the contour C. The function defined implicitly
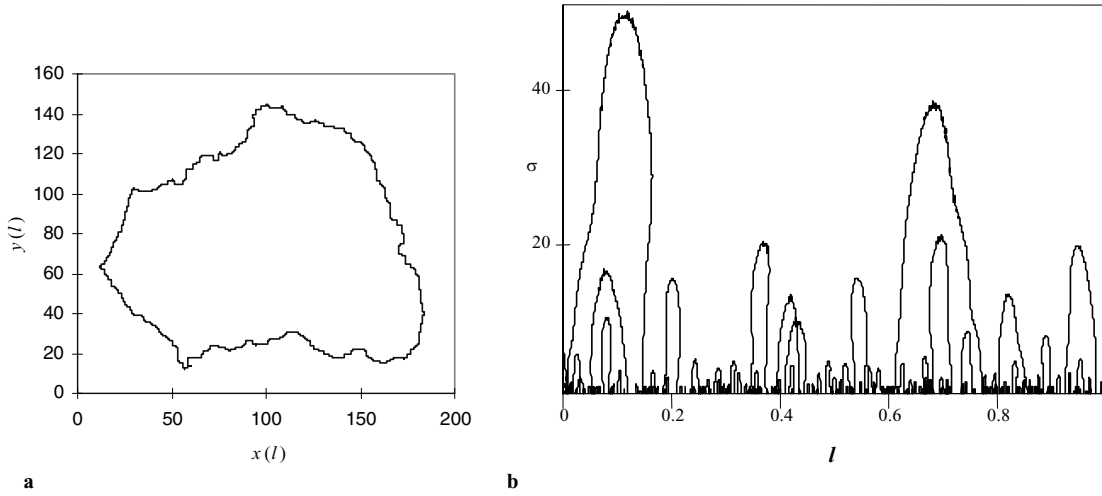
Figure 13.   (a) contour of a figure; (b) curvature scale space image of the contour.

by $\kappa(l, \sigma) = 0$ is the *curvature scale space image* of C. It can be represented graphically as a binary image (Fig. 13) in which each row corresponds to a specific value of σ and each column corresponds to a specific value of l. Often the normalized arc length parameter defined on [0, 1] is used instead of l.

The curvature scale space image of a contour is a convenient shape representation that can be useful in such applications as shape recognition and matching, overlapping objects shape extraction, etc. This representation is invariant under translation. Size changes of the figure result in re-sizing the corresponding curvature scale space image in the vertical direction, rotation itself of the figure changes nothing, but change of the starting point causes a circular shift of the corresponding curvature scale space image in horizontal direction whereas reflection of the figure results in reflection of its curvature scale space image. The function is very robust to noise, small distortions on the contour do not change corresponding curvature scale space image too much.

3.6. Continuous Wavelet Transform

Consider a contour function $f(x)$. Its *continuous wavelet transform* with respect to a wavelet mother function $\psi(x)$ is defined as [1, 23, 35, 39]

$$U(a, b) = \int_{-\infty}^{\infty} f(x)\psi_{(a,b)}(x)\, dx$$

where the wavelets used are in the form of Grossmann-Morlet wavelets:

$$\psi_{(a,b)}(x) = \frac{1}{\sqrt{a}}\psi\left(\frac{x - b}{a}\right) \text{ where } a > 0, b \in \text{R}.$$

Wavelets are functions $\psi : \text{R} \to \text{R}$ with the property that $\{\psi_{(p_1, p_2)}\}$ forms an orthonormal basis of $L^2(\text{R})$. Wavelet transform of a function $f(x)$ is the set of coefficients $U(a, b)$ (Fig. 14(a)). Behavior of the coefficients under the basic geometric transformations of the figure can be predicted as:

1. *translation*: $U[\psi; f(x) + z] = U[\psi; f(x)] + U[\psi; z] = U[\psi; f(x)]$
2. *scaling*: $U[\psi; cf(x/c)](a, b) = cU[\psi; f(x)](a/c, b/c)$
3. *rotation*: $U[\psi; e^{i\theta}f(x - x_0)](a, b) = e^{i\theta}U[\psi; f(x)](a, b - x_0)$

where $f(x)$, in the general case, is a complex function, $U[\psi; f(x)](a, b) \equiv U(a, b), z \in \text{C}, c \in \text{R}^+, x_0 \in \text{R}$ and $\theta \in [0, 2\pi]$. If a wavelet with compact support is used, then local modifications of the shape affect the wavelet representation only locally.

Different shape properties can be obtained from the wavelet representation. The basic idea of such shape analysis is to find the vertical maxima lines of the wavelet representation. The set of all vertical maxima lines is called the *skeleton* of the wavelet representation (Fig. 14(b)). The scale-space lifetime of each maxima line or, alternatively, their length can be used as a measure of their relevance. Most relevant maxima
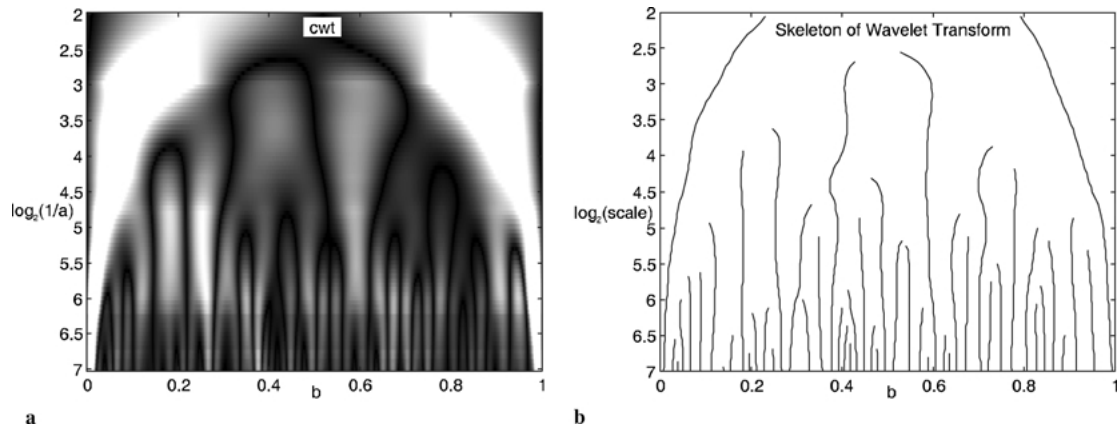
Figure 14. Wavelet analysis: (a) continuous wavelet transform (using 'Sombrero' wavelets) of the normalized tangent-angle function $\phi_X^*(t)$ shown in Fig. 10(b); (b) skeleton of the wavelet transform.

lines correspond to the dominant points (corners) on the analyzed contour.

3.7. Radon Transform

The Radon transform of a function $f(x, y)$ defined on figure X is defined as the integral of f over the line $\rho = x\cos(\theta) + y\sin(\theta)$ [28, 29, 49]

$$Rf(\rho, \theta)$$
$$= \iint f(x, y)\delta(\rho - x\cos(\theta) - y\sin(\theta))\, dx\, dy$$

where δ denotes Dirac δ-function, $\rho \in \mathbf{R}$, and $\theta \in [0, \pi)$. For shape analysis it is of particular interest to consider the case where

$$f(x, y) = \begin{cases} 1, & (x, y) \in c_X(l) = (x_X(l), y_X(l)) \\ 0, & \text{otherwise} \end{cases}$$
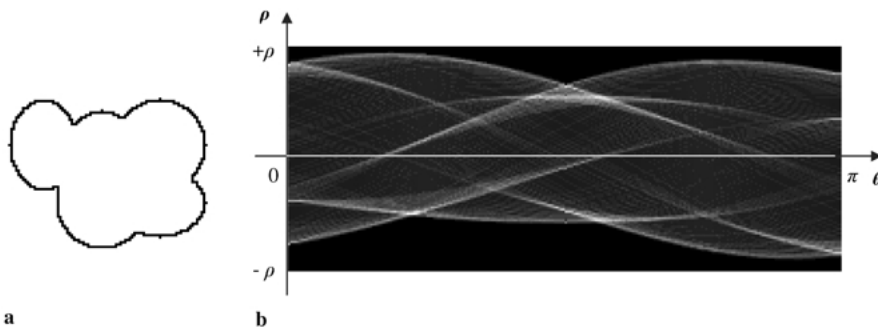
Behavior of the transform under basic geometric transformations of the figure can be predicted as [49]:

1. *translation*: $f(x, y) = g(x - x_0, y - y_0) \Rightarrow Rf(\rho, \theta) = Rg(\rho - x_0\cos\theta - y_0\sin\theta, \theta)$
2. *scaling*: $f(x, y) = g(x/a, y/b), a > 0, b > 0 \Rightarrow Rf(\rho, \theta) = ab|\gamma|^{-1} Rg(\tilde{\rho}, \tilde{\theta})$ where $\tilde{\rho} = \frac{\rho}{\gamma}$,

$$\tilde{\theta} = \begin{cases} \arctan(ba^{-1}\tan\theta) & \text{if } 0 \le \theta < \pi/2 \\ \arctan(ba^{-1}\tan\theta) + \rho & \text{if } \pi/2 \le \theta < \pi \end{cases},$$
$$\text{and } \gamma = \sqrt{(a\cos\theta)^2 + (b\sin\theta)^2}$$

3. *rotation*: $f(r, \phi) = g(r, \phi - \phi_0) \Rightarrow Rf(\rho, \theta) = Rg(\rho, \theta - \phi)$ where f and g are expressed in polar coordinates.

An example of the Radon transform is shown in Fig. 15. For shape analysis, 2D binary edge and accumulation maps are of the main interest as they allow one to obtain

Figure 15. Radon transform: (a) contour of a figure; (b) radon transform of the contour.

some vital shape properties. Thus, angularity can be defined as the average of the accumulated values on the bounding curve of the distribution at and on either side of a maximum value. For a shape with n protrusions, the average value should be taken as the angularity factor. Feret diameter, d_θ, for a particular orientation θ equals the distance between the opposite bounding curves on a 2D binary edge map at θ. The perimeter of the convex hull can be defined using the average Feret diameter, d_{av}, as $p_h = \pi d_{av}$. Consequently, convexity factor can be derived from the ratio of the convex hull perimeter and the number of image points which contribute to the convex hull. The number of lobes on the convex hull is obtained by counting the number of maxima on the bounding curve. Size factor and elongation ratio are among the other shape characteristics that can be calculated from the 2D binary edge map [29].

4. Concluding Remarks

There exist different classes of contour functions that are defined on different domains and have different properties and characteristics. Their commonality however is that the map $X \rightarrow f_X$ transforms figures into elements of a function space, thus allowing various tools developed for analyzing the functions to be used for analyzing the shape. This approach allows one to bring the problem of shape analysis to the level of abstraction present in the theory of functions, thus providing a uniform framework within which other shape functions can be introduced and analysis methodologies can be applied.

Various contour functions have certain advantages and limitations. Thus, the application of the cross-section function is limited only to symmetric figures, the radius-vector function requires the figure to be star-shaped, whereas for the support function convexity is desirable. The tangent-angle function, contour curvature, and contour complex functions as well as contour parametric functions can be applied to any contours. Most of the functions depend on the choice of a reference point and they behave differently under basic geometrical transformations such as translation, rotation, size changes, and reflection. Some of them are or can be defined on $[0, 2\pi]$ interval. Therefore, when choosing a particular contour function for a specific application, one should consider all the properties of the function and the ability to extract any additional useful parameters.

For the analysis of contour functions, many ideas of the function analysis as well as the differential and computational geometry techniques can be applied in addition to the techniques described above. Also, a contour function can be considered as a realization of a random process and the theory of stochastic models and statistical analysis can be used.

References

1. J. Antoine, D. Barache, R. Cesar Jr., and L. Costa, "Multiscale shape analysis using the continuous wavelet transform," in *Proc. IEEE ICIP'96*, 1996.
2. H. Bandemer, M. Albrecht, and A. Kraut, "On using Fourier series in characterizing particle shape," *Particle Characterization*, Vol. 2, pp. 98–103, 1985.
3. J. Beddow (Ed.), *Advanced Particulate Morphology*, Series in Fine Particle Science and Technology, Vol. 1, CRC Press: Boca Raton, 1980.
4. J. Beddow (Ed.), *Particle Characterization in Technology: Morphological Analysis*, CRC Press: Boca Raton, 1984.
5. R. Cesar Jr. and L. Costa, "Piecewise linear segmentation of digital contours in $0(N.\text{Log}(N))$ through a technique based on effective digital curvature estimation," *Real-Time Imaging*, Vol. 1, pp. 409–417, 1995.
6. R. Cesar Jr. and L. Costa, "Shape characterization in natural scales by using the multiscale bending energy," in *Proc. 13th ICPR*, Vol. I, pp. 735–739, 1996.
7. R. Cesar Jr. and L. Costa, "Shape characterization by using the Gabor transform," in *Proceedings of 7th IEEE DSP Workshop*, 1996, pp. 215–218.
8. G. Chuang and J. Kuo, "Wavelet description of planar curves: Theory and applications," *IEEE Trans. Image Process*, Vol. 5, pp. 56–70, 1996.
9. W. Dahmen, M. Gasca, and C. Micchelli (Eds.), *Computation of Curves and Surfaces*, NATO ASI Series, Series C: Mathematical and Physical Sciences, Kluwer Academic Publishers: Dordrecht, 1990.
10. A. Del Bimbo, M. De Marsico, S. Levialdi, and G. Perotore, "Query by dialog: An interactive approach to pictorial querying," *Image and Vision Computing*, Vol. 16, pp. 557–569, 1998.
11. E. Derbyshire, D. Unwin, X. Fang, and M. Langford, "The Fourier frequency-domain representation of sediment fabric anisotropy," *Computers and Geoscence*, Vol. 18, No. 1, pp. 63–73, 1992.
12. R. Duda and P. Hart, *Pattern Classification and Shape Analysis*. Wiley: New York, 1973.
13. R. Ehrlich and B. Weinberg, "An exact method for characterization of grain shape," *Journal of Sedimentology*, Vol. 40, No. 1, pp. 205–212, 1970.
14. G. Elber and M.-S. Kim, Geometric shape recognition of freeform curves and surfaces," *Graphical Models and Image Processing*, Vol. 59, No. 6, pp. 417–433, 1997.
15. J. Foley, A. Van Dam, S. Feiner, and J. Hughes, *Computer Graphics: Principles and Practice*, Addison-Wesley: New York, 1996, pp. 478–516.

16. S. Fong, J. Beddow, and A. Vetter, "A refined method of particle shape representation," *Powder Technology*, Vol. 22, pp. 17–21, 1979.

17. W. Full and R. Ehrlich, "Some approaches for location of centroids of quartz grain outlines to increase homology between Fourier amplitude spectra," *Mathematical Geology*, Vol. 14, No. 1, pp. 43–55, 1982.

18. C.-L. Huang and D.-H. Huang, "A content-based image retrieval system," *Image and Vision Computing*, Vol. 16, pp. 149–163, 1998.

19. A. Imiya, "Digital snakes," in *Proc. SPIE Vision Geometry IX*, 2000, Vol. 4117, pp. 24–35.

20. H. Ip and D. Shen, "An affine-invariant active contour model (AI-snake) for model-based segmentation," *Image and Vision Computing*, Vol. 16, pp. 135–146, 1998.

21. M. Jacob, T. Blu, and M. Unser, "An exact method for computing the area moments of wavelet and spline curves," *IEEE Transactions on Pattern Analysis and Machine Intelligence*, Vol. 23, No. 6, pp. 633–642, 2001.

22. A. Jain, *Fundamentals of Digital Image Processing*, Prentice-Hall International: Englewood Cliffs, 1989.

23. B. Jawerth and W. Sweldens, "An overview of wavelet based multiresolution analyses," *SIAM Rev.*, Vol. 36, No. 3, pp. 377–412, 1994.

24. V. Kindratenko and P. Van Espen, "Classification of irregularly shaped micro-objects using complex Fourier descriptors," in *Proc. 13th ICPR*, 1996, Vol. II, pp. 285–289.

25. J. Koplowitz and A. Bruckstein, "Design of perimeter estimator for digitized planar shapes," *IEEE Transactions on Pattern Analysis and Machine Intelligence*, Vol. 11, No. 6, pp. 611–622, 1989.

26. G. Lambert and H. Gao, "Line moments and invariants for real time processing of vectorized contour data," in *Lecture Notes in Computer Science*, Vol. 974, Springer-Verlag: Berlin, 1995, pp. 347–352.

27. G. Lambert and J. Noll, "Discrimination properties of invariants using the line moments of vectiruzed contours," in *Proceedings of 13th ICPR*, 1996, Vol. II, pp. 735–739.

28. V. Leavers, "Morphology and classification of powder particles using the Radon transform," *Part. Part. Syst. Charact.*, Vol. 17, pp. 66–76, 2000.

29. V. Leavers, "Use of the two-dimensional Radon transform to generalize a taxonomy of shape for the characterization of abrasive powder particles," *IEEE Transactions on Pattern Analysis and Machine Intelligence*, Vol. 22, No. 12, pp. 1411–1423, 2000.

30. H.-C. Liu and M. Srinath, "Partial shape classification using contour matching in distance transformation," *IEEE Transactions on Pattern Analysis and Machine Intelligence*, Vol. 12, No. 11, pp. 1072–1079, 1990.

31. S. Loncaric, "A survey of shape analysis techniques," *Pattern Recognition*, Vol. 31, No. 8, pp. 983–1001, 1998.

32. D. Luerkens, J. Beddow, and A. Vetter, "Morphological Fourier descriptors," *Powder Technology*, Vol. 31, pp. 209–215, 1982.

33. A. Mackworth and F. Mokhtarian, "The renormalized curvature scale space and the evolution properties of planar curves," in *Proc. of CVPR'88*, 1988, pp. 318–326.

34. J. Marshall (Ed.), *Clastic Particles: Scanning Electron Microscopy and Shape Analysis of Sedimentary and Volcanic Classes*, Van Nostrand Reinhold: New York, 1990.

35. Y. Meyer, *Wavelets: Algorithms and Applications*, Society for Industrial and Applied Mathematics, Philadelphia, 1993.

36. F. Mokhtarian, "Silhouette-based isolated object recognition through curvature scale space," *IEEE Transactions on Pattern Analysis and Machine Intelligence*, Vol. 17, No. 5, pp. 539–544, 1995.

37. F. Mokhtarian and A. Mackworth, "Scale-based description and recognition of planar curves and two-dimensional shapes," *IEEE Transactions on Pattern Analysis and Machine Intelligence*, Vol. 8, No. 1, pp. 34–43, 1986.

38. F. Mokhtarian and A. Mackworth, "A theory of multiscale, curvature-based shape representation for planar curves," *IEEE Transactions on Pattern Analysis and Machine Intelligence*, Vol. 14, No. 8, pp. 789–805, 1992.

39. Y. Nakamura, K. Satoda, and M. Nagao, "Shape description and matching using wavelet extrema," in *Proc. ACCV'93*, 1993, pp. 640–643.

40. E. Persoon and K.-S. Fu, "Shape discrimination using Fourier descriptors," *IEEE Transactions on Pattern Analysis and Machine Intelligence*, Vol. 8, No. 4, pp. 388–397, 1986.

41. J. Prince and A. Willsky, "Reconstructing convex sets from support line measurements," *IEEE Transactions on Pattern Analysis and Machine Intelligence*, Vol. 12, No. 4, pp. 377–389, 1990.

42. B. Raeymaekers, P. Van Espen, and F. Adams, "The morphological characterization of particles by automated scanning electron microscopy," *Microchimica Acta*, Vol. 2, pp. 437–454, 1984.

43. B. Ray and K. Ray, "Scale-space analysis and corner detection on digital curves using a discrete scale-space kernel," *Pattern Recognition*, Vol. 30, No. 9, pp. 1463–1474, 1997.

44. A. Rosenfeld and A. Nakamura, "Local deformations of digital curves," *Pattern Recognition Letters*, Vol. 18, pp. 613–620, 1997.

45. B. Shahraray and D. Anderson, "Optimal estimation of contour properties by cross-validated regularization," *IEEE Transactions on Pattern Analysis and Machine Intelligence*, Vol. 11, No. 6, pp. 600–610, 1989.

46. D. Stoyan and H. Stoyan, *Fractals, Random Shapes and Point Fields (Methods of Geometrical Statistics)*, John Wiley & Sons: Chichester, 1995.

47. J.-P. Tarel, "The complex representation of algebraic curves and its simple exploitation for pose estimation and invariant recognition," *IEEE Transactions on Pattern Analysis and Machine Intelligence*, Vol. 22, No. 7, pp. 663–674, 2000.

48. M. Thomas, R. Wiltshire, and A. Williams, "The use of Fourier descriptors in the classification of particle shape," *Sedimentology*, Vol. 42, pp. 635–645, 1995.

49. P. Toft, The Radon transform—theory and implementation, Ph.D. thesis, Technical University of Denmark, 1996.

50. T. Wallace and P. Wintz, "An effective three-dimensional aircraft recognition algorithms using normalized Fourier descriptors," *Computer Graphics and Image Processing*, Vol. 13, pp. 99–126, 1980.

51. M. Worring, *Shape Analysis of Digital Curves*, Febodruk, Enschede, 1993.

52. X. Wu and J. Rokne, "On properties of discretized convex curves," *IEEE Transactions on Pattern Analysis and Machine Intelligence*, Vol. 11, No. 2, pp. 217–223, 1989.

Volodymyr V. Kindratenko graduated in mathematics and computer science from the State Pedagogical University, Kirovograd, Ukraine, in 1993. He received Ph.D. degree from the University of Antwerp, Belgium, in 1997. His research involved the development and application of image analysis techniques for the identification and classification of microscopic particles. From 1997 to 1998, Volodymyr Kindratenko was employed by the University of Illinois as a Postdoctoral Research Associate in the Virtual Environments group.

He is now a Research Scientist at the National Center for Supercomputing Applications at the University of Illinois at Urbana-Champaign. Dr. Kindratenko is a member of IEEE and ACM. His current research interests include virtual reality, human-computer interaction techniques, sensors, and computer vision. He has been published in the areas of image processing and virtual reality.